Stem Cell Reports
Article

OPEN ACCESS

A Multi-Lineage Screen Reveals mTORC1 Inhibition Enhances Human Pluripotent Stem Cell Mesendoderm and Blood Progenitor Production

Emanuel Joseph Paul Nazareth,[1] Nafees Rahman,[1,2] Ting Yin,[1] and Peter William Zandstra[1,2,3,*]
[1]Institute of Biomaterials and Biomedical Engineering, University of Toronto, Toronto, ON M5S 3G9, Canada
[2]Department of Chemical Engineering and Applied Chemistry, University of Toronto, Toronto, ON M5S 3E5, Canada
[3]Medicine by Design, University of Toronto, Toronto, ON M5S 3G9, Canada
*Correspondence: peter.zandstra@utoronto.ca
http://dx.doi.org/10.1016/j.stemcr.2016.04.003

SUMMARY

Human pluripotent stem cells (hPSCs) exist in heterogeneous micro-environments with multiple subpopulations, convoluting fate-regulation analysis. We patterned hPSCs into engineered micro-environments and screened responses to 400 small-molecule kinase inhibitors, measuring yield and purity outputs of undifferentiated, neuroectoderm, mesendoderm, and extra-embryonic populations. Enrichment analysis revealed mammalian target of rapamycin (mTOR) inhibition as a strong inducer of mesendoderm. Dose responses of mTOR inhibitors such as rapamycin synergized with Bone Morphogenetic protein 4 (BMP4) and activin A to enhance the yield and purity of BRACHYURY-expressing cells. Mechanistically, small interfering RNA knockdown of RAPTOR, a component of mTOR complex 1, phenocopied the mesendoderm-enhancing effects of rapamycin. Functional analysis during mesoderm and endoderm differentiation revealed that mTOR inhibition increased the output of hemogenic endothelial cells 3-fold, with a concomitant enhancement of blood colony-forming cells. These data demonstrate the power of our multi-lineage screening approach and identify mTOR signaling as a node in hPSC differentiation to mesendoderm and its derivatives.

INTRODUCTION

Human pluripotent stem cells (hPSCs) and their differentiated derivatives offer the exciting opportunity to develop tools to study and treat human diseases. However, robust and reproducible control of hPSC fate remains challenging. Small molecules offer one approach to control hPSC fate, and the discovery and characterization of these compounds can be facilitated by cell-based phenotypic high-throughput screening (HTS). Emerging data from hPSC assays has revealed variable and contradictory observations, even with matched cell lines and protocols (Haibe-Kains et al., 2013). Although the factors underlying this variability are not completely known, population context has been identified as a main contributor to assay inconsistency (Snijder et al., 2012). Spatially heterogeneous (Peerani et al., 2007) micro-environmental factors such as endogenous ligands, extra-cellular matrix proteins (ECMPs), and cell subpopulations are strong regulators of hPSC fate. Specifically, spatial cell distribution has been shown to affect hPSC self-renewal (Maherali and Hochedlinger, 2008), differentiation trajectories in both normal and patient-derived cells (Cai et al., 2009; Chambers et al., 2009), and disease phenotypes (Sun et al., 2012).

Consequently, robust assays that combine defined culture conditions with comprehensive analysis of cell responses to exogenous cues are needed. To this end, we developed a chemically defined cell patterning-based high-throughput (HTP) assay, engineering colony size, local cell density, medium composition, and substrate for rapid and robust measurement of hPSC fate responses to exogenous cues (Nazareth et al., 2013). We applied the assay to screen a library of kinase inhibitors for effects on four early hPSC fates. For each compound, the change in yield and purity in the resulting pluripotent, neuroectoderm (NE), mesendoderm, and extra-embryonic populations were simultaneously tracked, allowing for estimation of selection and induction events. Our analysis identified mammalian target of rapamycin (mTOR) inhibitors, such as rapamycin, as having a strong mesendoderm-inducing effect on hPSCs. Rapamycin was subsequently shown to synergize with bone morphogenetic protein 4 (BMP4) and activin A to enhance BRACHYURY induction more than 3-fold, an effect that propagated to equivalent enhancements of hemogenic endothelium and blood progenitor cells. This study demonstrates the advantages of controlling micro-environmental parameters and measuring multiple subpopulation outputs in parallel on PSC fate screening assays. This strategy should enhance discovery in more complex and predictive multi-cell population drug-screening assays.

RESULTS

A Kinase Inhibitor Screen of hPSCs Revealed Lineage-Specific Regulators

We previously developed a 48-hr hPSC screen that employs control of spatial cell patterning to configure the hPSC micro-environment for rapid and robust response

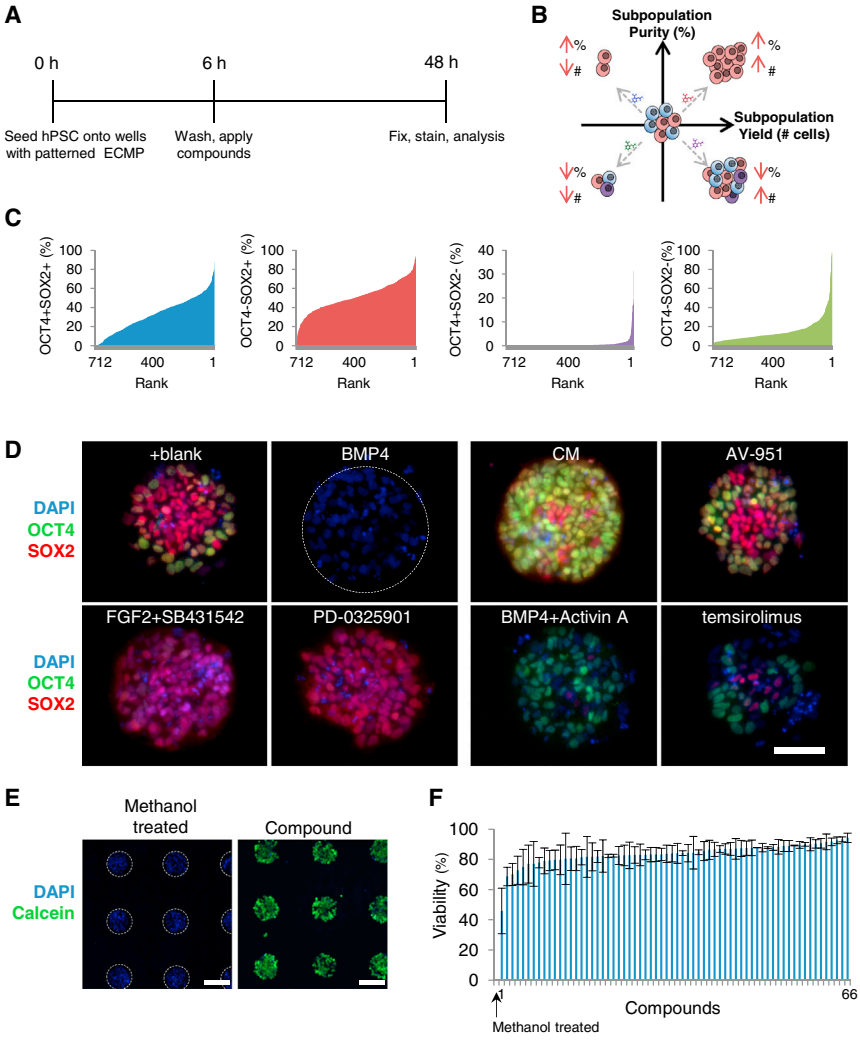

Figure 1. HTS of Small-Molecule Regulators of hPSC Pluripotency, Primitive Streak, NE, and Extra-embryonic/Other Cell-Fate Decisions

(A) Assay design. hPSCs are micro-patterned on micro-contact printed 200-μm diameter extracellular matrix proteins (ECMP) circles in 96-well plates. Control or base medium with test compounds is added to each well. After 48 hr, imaging is performed and single-cell OCT4 and SOX2 expression levels are quantified.

(B) Subpopulation purity and high yield are measured to determine inductive effects of compounds. Diagram demonstrates the changes in composition and purity of the "pink" cell population.

(C) Compound distribution ranked by induction efficiency of pluripotency, NE, primitive streak, and extra-embryonic/other cell fates.

(D) Sample composite colony images from controls and selected responders stained for DNA (DAPI, blue), OCT4 (green), and SOX2 (red). BMP4 is the $OCT4^{-}SOX2^{-}$ control, CM is the $OCT4^{+}SOX2^{+}$ control, FGF2 + SB431542 is the $OCT4^{-}SOX2^{+}$ control, and BMP4 + activin A is the $OCT4^{+}SOX2^{-}$ control. Colony outlined with dotted white line. Scale bar, 100 μm.

(E) Calcein (viability) staining of unfixed cells at 48 hr treated with hit compounds. Non-viable control treated with methanol. Colonies are outlined with a dotted white line. Scale bar, 200 μm.

(F) 67 putative hit compounds ranked by increasing viability. n = 3 independent biological replicates. Error bars indicate SD.

See also Figure S1.

to exogenous cues (96μCP assay) (Nazareth et al., 2013) (Figure 1A). Single-cell OCT4 and SOX2 costaining enables simultaneous classification of pluripotent ($OCT4^{+}SOX2^{+}$), NE ($OCT4^{-}SOX2^{+}$), mesendoderm ($OCT4^{+}SOX2^{-}$), and extra-embryonic/other ($OCT4^{-}SOX2^{-}$) cell fates. This platform can be used to screen test factor effects on yield (percentage) and purity (absolute number of cells) of each subpopulation per colony using in-house software (Figure 1B).

We applied this platform to screen a collection of 400 small-molecule kinase inhibitors at two concentrations (0.2 μM and 1 μM). To ensure a significantly large sample size, we performed further analysis only on compounds which yielded >800 imaged cells per well, resulting in 707 unique conditions including five controls on each plate: base medium (blank), PSC supporting mouse embryonic fibroblast (MEF)-conditioned (CM), NE inducing transforming growth factor β (TGF-β) inhibitor and fibroblast growth factor 2 (FGF2) (TiF), mesendoderm inducing BMP4 with activin A (BA), and extra-embryonic inducing BMP4. The overall distributions of the compounds with respect to each subpopulation indicated that mesendoderm and extra-embryonic/other inducing compounds were underrepresented (Figure 1C). Control conditions showed high reproducibility across plates (Figure S1A). Calculation of the Z′ factor, a statistical parameter used to compare HTP assays (Zhang et al., 1999), for the pattern-based (Z′ = 0.94)and non-pattern-based (Desbordes et al., 2008) (Z′ = 0.29, $p < 0.01$) assays supported the rationale for controlling micro-environments to improve robustness (Figures S1B and S1C). Sample images of control conditions and select responders are shown in Figure 1D. Viability of endpoint cells was confirmed at 48 hr using calcein and Hoechst staining (Figures 1E and 1F).

To visualize factor effects on responding population cell yield and purity, we measured the percentage and average

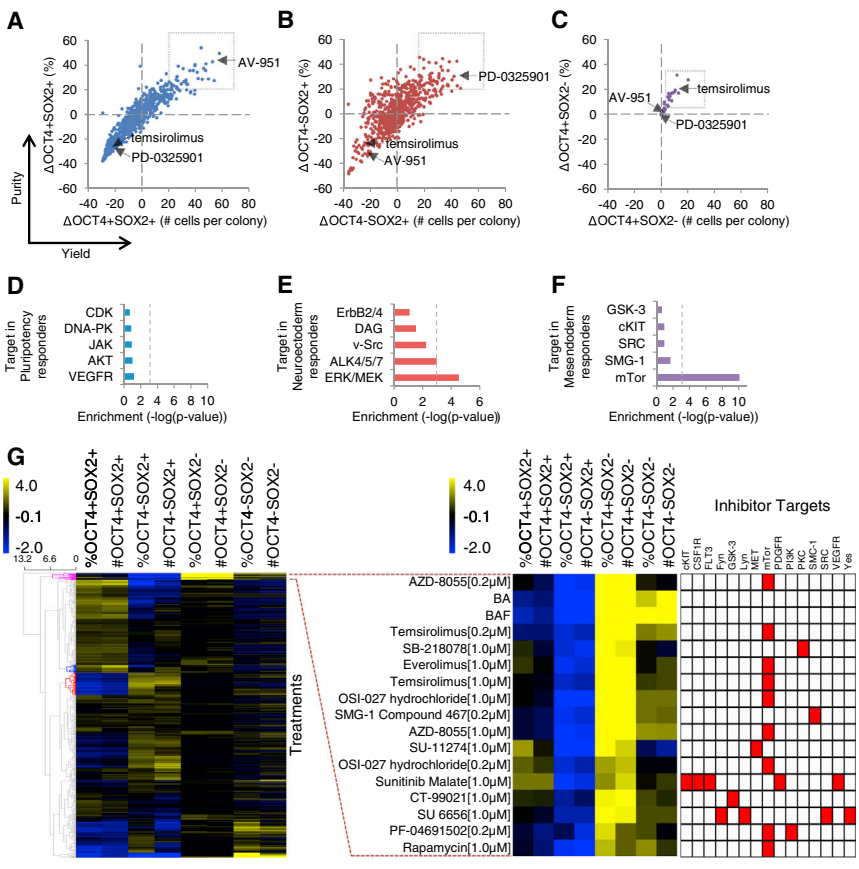

Figure 2. Pathway Enrichment Analysis

(A) Increase in PSC purity (%OCT4$^+$SOX2$^+$) versus increase in yield (number of OCT4$^+$ SOX2$^+$ cells per colony) obtained from 712 unique treatments. Values from blank were subtracted (graph origin represents base medium alone). Thresholds for purity and yield were used to classify "pluripotency responders." Arrow indicates a sample responding compound.

(B and C) Similar analysis as in (A) to classify (B) NE and (C) mesendoderm responders. Dotted lines outline the regions classified as responders.

(D) Enrichment in PSC responders (shown in Figure 1D). p Values were obtained for each target, using the hypergeometric distribution, and shown in −log base 10. Threshold corresponds to p = 0.001.

(E and F) Similar analysis as in (D) for (E) NE and (F) mesendoderm responders.

(G) Two-dimensional hierarchical clustering of subpopulation yield and purity data across treatments. Left: sample similarity tree, with samples clustered. Enhanced primitive streak cluster is in purple, PSC cluster in blue, and NE cluster in red. Right: detailed view of enhanced primitive streak cluster, indicating compound name, concentration, and reported kinase targets indicated in red.

See also Figures S2 and S3; Table S2.

number of cells of each subpopulation per colony per well. For example, to visualize effects on the PSC population we subtracted the percentage and number of OCT4$^+$SOX2$^+$ cells obtained in the blank to obtain ΔOCT4$^+$SOX2$^+$ (%) and ΔOCT4$^+$SOX2$^+$ (number of cells per colony), respectively (Figure 2A). Based on the subpopulation positive controls, we set thresholds for yield and purity to obtain a list of "responders." Similar visualizations are shown for NE (OCT4$^-$SOX2$^+$) (Figure 2B) and mesendoderm (OCT4$^+$SOX2$^-$) (Figure 2C). Enlarged plots of the threshold regions showing compound names of responders are shown in Figure S2. Visual inspection of responding compounds confirmed the expected yield and purity effects (Figure 1D). Based on these results, we sought to determine whether responding compounds were enriched for specific inhibitor targets.

Specific Kinase Inhibitor Targets for NE and Mesendoderm Induction Identified

To identify fate-modulating pathways enriched in our library, we performed a hypergeometric test to obtain p values for the enrichment of each kinase target in the PSC, NE, and mesendoderm responder groups (five most enriched targets are shown in Figures 2D–2F; count of unique compounds for each kinase target is shown in Figure S3A; count of kinase targets in responders and total screen is shown in Table S1). For the PSC-enhanced cluster no target family was statistically enriched, indicating that the tested kinase inhibitors do not robustly rescue hPSCs from differentiation in the blank lacking exogenous FGF2 and activin A (Vallier et al., 2005). This suggests that, in contrast to differentiation, exogenous pathway agonists, or a combination of inhibitors, may be required to maintain pluripotency in vitro (Tsutsui et al., 2011). For NE responders we obtained the highest enrichment for small molecules targeting the ERK/MEK pathway ($p = 2.9 \times 10^{-5}$) (Figure 2E), as well as a high enrichment ($p = 0.001$) of small molecules targeting TGF-β superfamily type I activin receptor-like kinase (ALK) receptors ALK4, ALK5, and ALK7. Inhibition of TGF-β signaling has been well established to result in hPSC differentiation to NE (Smith et al., 2008; Vallier et al., 2004). We previously observed low levels of endogenous TGF-β signaling in the 96μCP assay, which likely contributes to lower than expected significance of ALK4/5/7 inhibitors. Lastly, in the mesendoderm responders

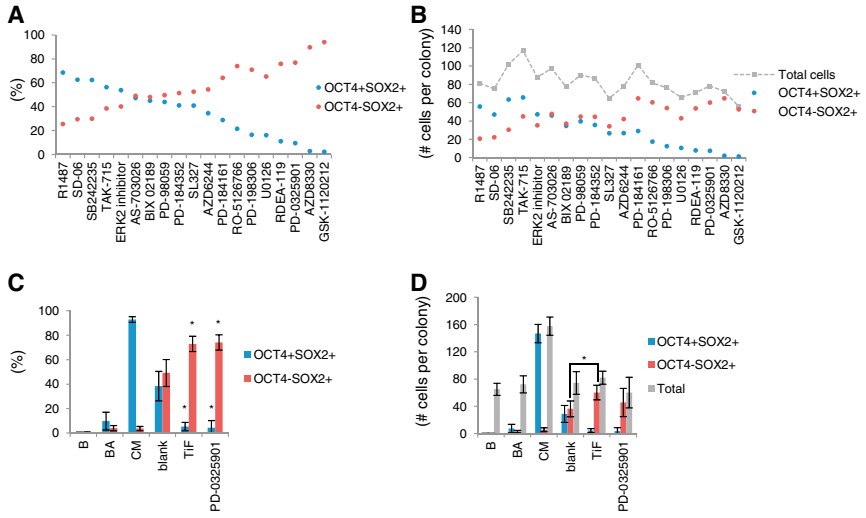

Figure 3. PSC and NE Subpopulation Screen Analysis

(A) Subpopulation percentages from all screened MEK/ERK inhibitors, ranked by PSC percentage response.

(B) Subpopulation cells per colony from all screened MEK/ERK inhibitors, ranked by PSC percentage response.

(C) The MEK inhibitor PD-0325901 increases the percentage of early NE and decreases the percentage of PSCs. *$p < 0.001$, significant difference from blank control; $n \geq 3$ independent biological replicates.

(D) MEK inhibitor PD-0325901 does not increase the number of early NE. *$p < 0.01$, significant difference from blank control; $n \geq 3$ independent biological replicates.

Error bars indicate SD. See also Figure S4.

we found the highest enrichment for mTOR inhibitors ($p = 8.1 \times 10^{-11}$) (Figure 2F).

In addition to target enrichment analysis, two-dimensional hierarchical clustering (707 conditions, eight outputs, 5,656 data points) revealed several distinct phenotype clusters (Figure 2G, left). A cluster of compounds that enhanced PSC (blue dendrogram) also contained the CM control (Figure S3B). Similarly, a cluster that enhanced NE (red dendrogram) also contained the TiF control (Figure S3C). The few compounds that enhanced mesendoderm (purple dendrogram) clustered with two mesendoderm induction controls, BA and BA with FGF2 (BAF) (Figure 2G, right). In this cluster, 53% of the compounds targeted mTOR and no other kinase was targeted by more than one compound. Enrichment analysis of the three clusters revealed identically significantly enriched pathways as our threshold-based method (Figure S3D), further confirming the ERK/MEK and mTOR enrichments found in the screen. Based on these results we sought to further validate the ERK/MEK and mTOR results.

ERK/MEK Inhibition Induces hPSC Differentiation to NE in a BMP-Dependent Manner

Analyzing all the ERK/MEK inhibitors in our library, we observed a general increase in the percentage of NE cells at the expense of PSCs, with no changes in total cell number (Figures 3A and 3B). To further investigate the effect of MEK inhibition, we retested PD0325901 and found a significant reduction in PSC yield and increase in NE frequency (both $p < 0.001$) (Figure 3C), but found no significant increase in NE cells per colony induced relative to the blank control ($p = 0.43$), indicative of selection (Figure 3D). Reports are mixed on the effects of MEK inhibition (via PD0325901) on neural induction, and there is strong evidence that variability in endogenous factors such as BMP has hindered interpretation of these previous results (Greber et al., 2011).

To further investigate, we performed a meta-analysis of a previous dataset of the response of a panel of cell lines to a set of conditions including blank medium, PD0325901, and TiF, using the 96μCP assay (Nazareth et al., 2013). This analysis demonstrated that PD0325901 and TiF variably induce early NE in a cell-line- and passage-dependent manner (Figure S4A). Next, to determine the dependencies of PD0325901-induced NE on other pathways, we compared the effect of PD0325901 on NE induction in the blank, with BA, or with 17 other single factors that are agonists or antagonists of major developmental pathways. When BMP4 was added with PD0325901, NE induction was reduced from 95% to less than 0.5% ($p < 0.002$), confirming that NE is exceptionally sensitive to BMP4, strengthening the possibility that endogenous BMP4 abolishes NE induction (Figure S4B). Notably, PD0325901 induction of NE was affected by other factors, including FGF2, activin A, TGF-β, insulin-like growth factor 1, and heregulin β1, congruent with previous proposals that inhibition of MEK, BMP, and TGF-β signaling (Greber et al., 2011) or dual BMP and TGF-β signaling (Kim et al., 2010) may indeed robustly induce NE regardless of variations in endogenous signaling. Together, these data confirm that NE induction via MEK inhibition alone is highly variable across hPSC lines, support our hypothesis that this induction is sensitive to BMP inhibition, and demonstrate that our platform can reveal subtle molecular perturbations of PSC fate.

mTOR Inhibitors Dose-Dependently Induce Mesendoderm in hPSCs

Our analysis indicated a strong effect of mTOR inhibition on mesendoderm induction. Conflicting reports show

that mTOR inhibition inhibits PSCs and enhances serum-mediated differentiation toward mesoderm and endoderm (Zhou et al., 2009), or may enhance the purity of pluripotent cells (Easley et al., 2010). To validate that mTOR inhibitors enhance mesendoderm induction, we screened nine mTOR inhibitors at both 1 μM and 0.1 μM, and screened eight inhibitors of additional pathways implicated in hPSC regulation. Ranking the compounds according to level of effect on mesendoderm induction (%OCT4$^+$SOX2$^-$), the mTOR inhibitors clearly separated from the others and the majority of conditions tested significantly enhanced the percentage of OCT4$^+$SOX2$^-$ cells relative to blank serum-free (SF) medium alone ($p < 0.05$) (Figure 4A). Rapamycin at 1 μM was the strongest responder of all the conditions, comparable with the BA control. Rapamycin binds to FKBP12 and inhibits the kinase activity of mTOR complex 1 (mTORC1), which contains mTOR and RAPTOR (Sabers et al., 1995). A separate complex containing mTOR and RICTOR (mTORC2) is thought to be rapamycin insensitive, although this is cell-line and context dependent (Lamming et al., 2012). In contrast to rapamycin and its derivatives such as temsirolimus and everolimus, which only target mTORC1, next-generation dual mTORC1/2 inhibitors have been developed, such as AZD-8055 and KU-63794. Notably, within the 18 mTOR inhibitor treatments (nine compounds at two concentrations), the top half of ranked responders are enriched for compounds only targeting mTORC1 ($p < 0.005$).

To further validate the effect of mTOR inhibitors on hPSCs, we performed ten-point dose curves of two mTOR inhibitors, rapamycin and AZD-8055, and again measured the four early OCT4/SOX2 subpopulations. As expected, both compounds increased the percentage of mesendoderm cells in a dose-dependent manner (Figure 4B). Surprisingly, a bimodal response to rapamycin was observed in the PSC response, where at 0.001 and 0.01 nM there was a moderate but significant enhancement of the percentage and number of PSCs. This enhancement was not seen at concentrations above 0.1 nM, where mesendoderm induction peaks at 0.1 μM (Figure 4C). The yield, and not just percentage, of PSCs are enhanced by low concentrations of rapamycin (Figure 4D). This bimodal response was seen with two additional replicates of rapamycin (not shown) but was not seen with AZD-8055, which may indicate that the mechanism is via mTORC1 inhibition (Figure 4D). Additional studies are required to understand this effect more completely.

mTOR Inhibitor-Mediated Induction of Mesendoderm Is BMP-Receptor and TGF-β-Receptor Dependent

To gain insight into the mechanism behind mTOR inhibition inducing mesendoderm in hPSCs, we screened 14 agonists and antagonists of early development signaling pathways, alone and with rapamycin (Figures 4E and S5). TGF-β1 and FGF2 moderately enhanced rapamycin-induced mesendoderm. Inhibition of either phosphatidylinositol-3-kinase (using LY-294002), a downstream effector of mTOR implicated in mesendoderm differentiation (Singh et al., 2012), or Wnt (using IWP4) did not significantly alter the effect of rapamycin. The effects of rapamycin were abolished by the BMP type I receptor (ALK2/3) inhibitor LDN-193189, MEK inhibitor PD-032591, and TGF-β receptor (ALK4/5/7) inhibitor SB-431542. Consistent with our results, MEK inhibition has been shown to divert differentiation from mesendoderm (Yu et al., 2011), indicating that mTOR inhibition is insufficient to overcome this effect. The LDN-193189 and SB-431542 results imply that rapamycin's effect on mesendoderm is dependent on BMP and TGF-β receptor-mediated signaling, which are both required for hPSC differentiation toward mesendoderm (Vallier et al., 2009). Addition of either (or both) of these inhibitors to rapamycin, relative to rapamycin alone, results in loss of the OCT4$^+$SOX2$^-$ population, no difference in the OCT4$^+$SOX2$^+$ population, and a moderately enhanced SOX2$^+$OCT4$^-$ population (Figure S5A), with no change in the total number of cells per colony (Figure S5B).

Based on the blocking effects of SB-431542 and LDN-193189, we reasoned that rapamycin, which induces mesendoderm alone in SF-defined medium, may act additively or synergistically with endogenous TGF-β/BMP signaling. We therefore generated a rapamycin dose curve with (rap+BA) and without (rap+BA) exogenous BMP4 (10 ng ml^{-1}) and activin A (100 ng ml^{-1}), and analyzed mesendoderm induction by BRACHYURY (Zhang et al., 2008) expression. The percentage and number of BRACHYURY$^+$ cells in both rap+BA and rap+BA increased in a rapamycin dose-dependent manner. The maximum percentage of BRACHYURY$^+$ cells achieved with rapamycin alone (19%) was comparable with the percentage achieved with BA alone (18%); however, rap+BA resulted in a more than 3-fold increased yield of BRACHYURY$^+$ (57%) compared with BA alone ($p < 0.005$) (Figure 4F). The number of BRACHYURY$^+$ cells per colony was also enhanced in rap+BA relative to BA alone by 3.8-fold ($p < 0.005$) (Figure 4G). Sample images are shown in Figure 4H. Similar trends were observed in dose curves generated from non-patterned hPSCs with rapamycin, or an alternative mTOR inhibitor (temsirolimus) and a BA background (Figures S5C–S5F).

Knockdown of RAPTOR Phenocopies the Mesendoderm-Inducing Effects of Rapamycin

Functionally, mTOR operates as part of two protein complexes, mTORC1 and mTORC2 (reviewed in Sabatini, 2006), which are differentially regulated by upstream

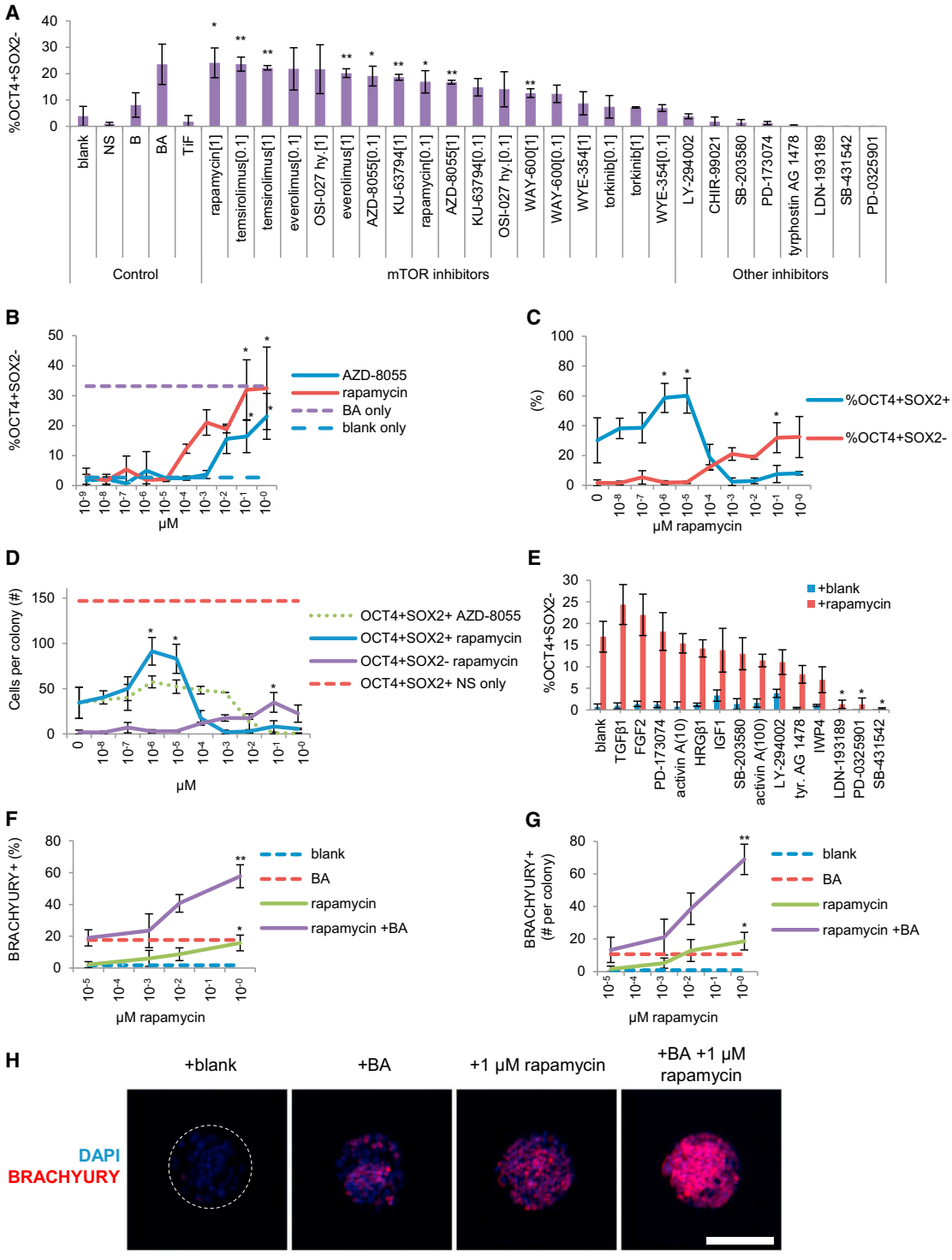

Figure 4. mTOR Inhibitors in Defined Medium Upregulate Mesendoderm via TGF-β and BMP Pathways

(A) Nine mTOR inhibitors in the OICR library were tested at 1 and 0.1 μM. Additional inhibitors of kinases implicated in early development but not targeting mTOR ("other inhibitors") were also tested. Small molecules were ranked by effect magnitude to separate mTOR inhibitors from others. *$p < 0.01$, **$p < 0.001$ compared with blank; n = 3 independent biological replicates.

(B) Ten-point dose curves of mTOR inhibitors rapamycin and AZD-8055 show a dose-dependent increase of % mesendoderm. *$p < 0.05$ compared with blank control; n = 3 independent biological replicates. Blank and BA response shown as reference lines.

(legend continued on next page)

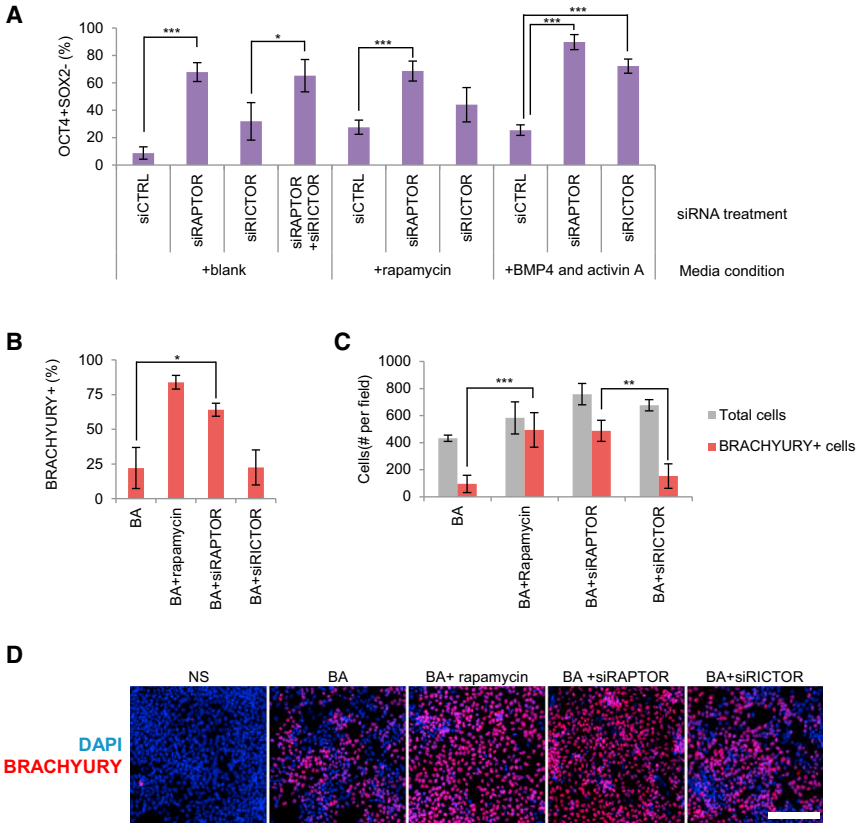

Figure 5. mTOR Inhibition Synergizes with BMP4 and Activin A in Inducing Mesendoderm

(A) The effect of siRNA on OCT4$^+$SOX2$^-$ mesendoderm. siRNA was applied to non-patterned hPSCs in different medium conditions as noted. *$p < 0.05$, ***$p < 0.0005$; n = 3 independent biological replicates.

(B) The effect of siRNA on BRACHYURY expression. siRNA was applied in different medium conditions as noted to non-patterned hPSCs. *$p < 0.05$; n = 4 independent biological replicates.

(C) Same experiment as in (B), showing number of BRACHYURY$^+$ cells per field and total cells. **$p < 0.005$, ***$p < 0.0005$; n = 4 independent biological replicates.

(D) Images of cells stained for DNA (DAPI, blue) and BRACHYURY expression (red), with treatments as indicated. Scale bar, 500 μm. Error bars indicate SD.

signals and have different downstream effectors. Although rapamycin was long thought to inhibit mTORC1, recent studies revealed that rapamycin can also inhibit mTORC2 in a cell-type-dependent manner (Lamming et al., 2012). To examine the role of each mTOR complex in rapamycin-induced mesendoderm differentiation, we targeted RAPTOR (mTORC1 specific) and RICTOR (mTORC2 specific) with small interfering RNA (siRNA). PSCs were seeded in pluripotency medium with siRNA against either RAPTOR (siRAPTOR) or RICTOR (siRICTOR). Two days after seeding, the medium was exchanged with fresh medium under three conditions (+blank, +rapamycin, or +BA), in the presence of siRNA. Analysis of OCT4 and SOX2 expression was conducted at day 4 (Figure 5A). In blank medium, siRAPTOR enhanced the percentage of mesendoderm (OCT4$^+$SOX2$^-$) cells relative to control scrambled siRNA (siCTRL) ($p < 0.0005$), but siRICTOR had no significant effect. Addition of both siRAPTOR and siRICTOR gave a phenotype similar to siRAPTOR alone, and gave rise to a significantly higher percentage of mesendoderm cells than siRICTOR alone ($p < 0.05$). In the presence of rapamycin, siRAPTOR again had a significant effect

(C) Ten-point dose curves of rapamycin show a bimodal increase in % PSCs. *$p < 0.05$ compared with blank (0 rapamycin); n = 3 independent biological replicates.

(D) Ten-point dose curves of rapamycin and AZD-8055 effect on number of PSCs per colony at subnanomolar concentrations of rapamycin but not AZD-8055. *$p < 0.05$ compared with blank (0 rapamycin); n = 3 independent biological replicates.

(E) 14 factors (ligands and small molecules) targeting early development pathways tested alone and with rapamycin to screen for interactions. n = 3 independent biological replicates. *$p < 0.05$, compared with blank + rapamycin condition.

(F) Dose curves of rapamycin performed alone and with BMP4 (10 ng ml^{-1}) and activin A (100 ng ml^{-1}) showing average percentage of BRACHYURY$^+$ cells per well was quantified. *$p < 0.05$ and **$p < 0.005$ both compared with the equivalent condition without rapamycin; n = 3 independent biological replicates. Response to blank and BMP4 and activin A alone ("BA") are shown as reference lines.

(G) Same experiment as in (F) showing the number of BRACHYURY cells per colony. *$p < 0.05$, **$p < 0.005$ compared with the equivalent condition without rapamycin; n = 3 independent biological replicates.

(H) Images of cells stained for DNA (DAPI, blue) and BRACHYURY expression (red), with treatments as indicated. Colony outlined with dotted white line. Scale bar, 200 μm.

Error bars indicate SD. See also Figure S5.

($p < 0.0005$), and siRICTOR was not significantly different from siCTRL. This result indicates that rapamycin (at 0.1 μM) is not completely inhibiting mTORC1. In the presence of BA, siRAPTOR also enhances the percentage of $OCT4^+SOX2^-$ cells relative to siCTRL ($p < 0.0005$). Interestingly, in this medium condition siRICTOR also enhanced the percentage of $OCT4^+SOX2^-$ ($p < 0.0005$), indicating that the effect of mTORC2 inhibition is dependent on TGF-β/BMP signaling. Focusing on the BA conditions, we repeated the siRNA assay and stained for BRACHYURY. As expected, siRAPTOR significantly enhanced both percentage (Figure 5B) and number (Figure 5C) of $BRACHYURY^+$ cells, similarly to rapamycin treatment. Sample images are shown in Figure 5D. No effect was observed from siRICTOR on BRACHYURY induction, indicating that the effect of rapamycin on BRACHYURY induction is primarily through mTORC1 and not mTORC2. These results also indicate a divergence between the $OCT4^+SOX2^-$ readout and BRACHYURY expression and further corroborate that rapamycin is acting via inhibition of mTOR signaling, not via non-specific effects.

mTOR Inhibition Impedes Endoderm and Enhances Mesoderm Differentiation

Based on the observation that mTOR inhibition enhances the purity and number of mesendoderm cells, we investigated the effect of rapamycin on specific downstream mesoderm and endoderm progenitors. We first differentiated hPSCs, in either BA or rap+BA (0.1 μM) for 42 hr, and assessed various markers of NE (*PAX3*, *PAX6*), mesendoderm (*MIXL1*, *BRACHYURY*), mesoderm (*MEIS1*, *MYB*), cardiac precursor (*MESP1*, *NKX2.5*, *PDGFRa*), hematopoietic (*RUNX1*), definitive endoderm (*EOMES*), primitive endoderm (*GATA6*, *AFP*), and trophectoderm (*HAND1*) lineages via qRT-PCR (Figure S6A). In general, rapamycin supplementation enhanced all differentiated lineage markers, with the exception of *HAND1*, a marker of trophectoderm, and *EOMES*, associated with definitive endoderm (DE).

We next specifically tested the effect of rapamycin on DE induction. Differentiation to DE is a multi-step process including a 1-day induction phase (D0) where cells are exposed to activin A (100 ng ml^{-1}) and the glycogen synthase kinase 3β (GSK3β) inhibitor CHIR99021 (CHIR, 2 μM) (Rezania et al., 2012). We tested various concentrations of rapamycin at D0 and measured the resulting $FOXA2^+SOX17^+$ DE at day 5. Although DE differentiation protocols can be extremely efficient in specific cell lines (Nostro et al., 2011), differentiation efficacy is known to vary greatly between different cell lines (Nazareth et al., 2013). Thus we tested four cell lines with varying DE induction efficiencies and demonstrated that rapamycin dose-dependently reduced DE induction (%$FOXA2^+SOX17^+$ cells) in PDX1, HES2, and HES3-RUNX1-GFP cell lines, and had no effect on H9 DE induction (Figure 6A). These results show that rapamycin does not enhance endoderm differentiation and may be specific to mesoderm induction.

Next, to test the effect of mTOR inhibition on mesoderm-derived lineages, we evaluated hematopoietic differentiation of hPSCs. During embryogenesis, hematopoietic cells are derived from specialized endothelial cells called hemogenic endothelium (HE), isolated using vascular endothelial cadherin (VECAD) and CD34 expression (Eilken et al., 2009). To track HE induction in our studies, hPSC (HES3-RUNX1-GFP cell line) aggregates were cultured in chemically defined medium (Pick et al., 2007) in the presence of rapamycin (0.1 μM) from day 0 to 2 and $VECAD^+CD34^+$ expression was assessed throughout an 8-day time course. Controls were cultured in the absence of rapamycin. The $CD34^+VECAD^+$ expression profile revealed that rapamycin addition from day 0 to day 2 enhances both purity and yield of HE (Figures 6B and 6C). Note that day-6 rapamycin-generated $CD34^+VECAD^+$ cells were also $CD73^-$ and $CD184^-$ (Figures S6B and S6C), further confirming their HE phenotype (Ditadi and Sturgeon, 2015). The maximum $CD34^+VECAD^+$ percentage reached in controls was 10% ± 4%, falling within the range of previously reported results in the literature (Ditadi and Sturgeon, 2015), whereas in rapamycin 30% ± 11% purity was attained ($p < 0.05$) (Figure 6D). Rapamycin addition also enhanced HE purity in the HES2 cell line (Figure S6D), demonstrating that our observations are not limited to the HES3-RUNX1-GFP line. Moreover, rapamycin conditions exhibited a 4-fold increase in $CD34^+VECAD^+$ cells on day 6 and a 2.5-fold increase on day 8 (99% confidence intervals shown in Figure 6E). Furthermore, kinase insert domain receptor (KDR, also known as vascular endothelial growth factor receptor 2) expression, an early marker of all blood cells (Shalaby et al., 1997), nearly doubled on day 4 in rapamycin (Figure S6E). To functionally assess whether early rapamycin treatment enhances blood progenitor induction, we seeded cells from cultures initiated either in the presence or absence of rapamycin in methylcellulose colony-forming cell (CFC) assays (Csaszar et al., 2012). A 1.7-fold increase ($p < 0.05$) in the number of CFCs per 10^5 cells was obtained in rapamycin-treated conditions (202 ± 42 CFCs [mean ± SEM]) compared with control conditions (117 ± 26 CFCs) (Figures 6F and S6F). Additionally, gene expression analysis at days 0, 1, and 2 confirmed that rapamycin addition significantly increased the expression of *BRACHYURY* ($p < 0.002$) and *MIXL1* ($p < 0.0002$) (Figure S6G). These results demonstrate that rapamycin treatment during days 0 to 2 of hematopoietic differentiation of hPSCs enhances the blood progenitor phenotype. A summary of our findings on the role of mTORC1 in hPSC lineage-fate decisions is presented in Figure 6G.

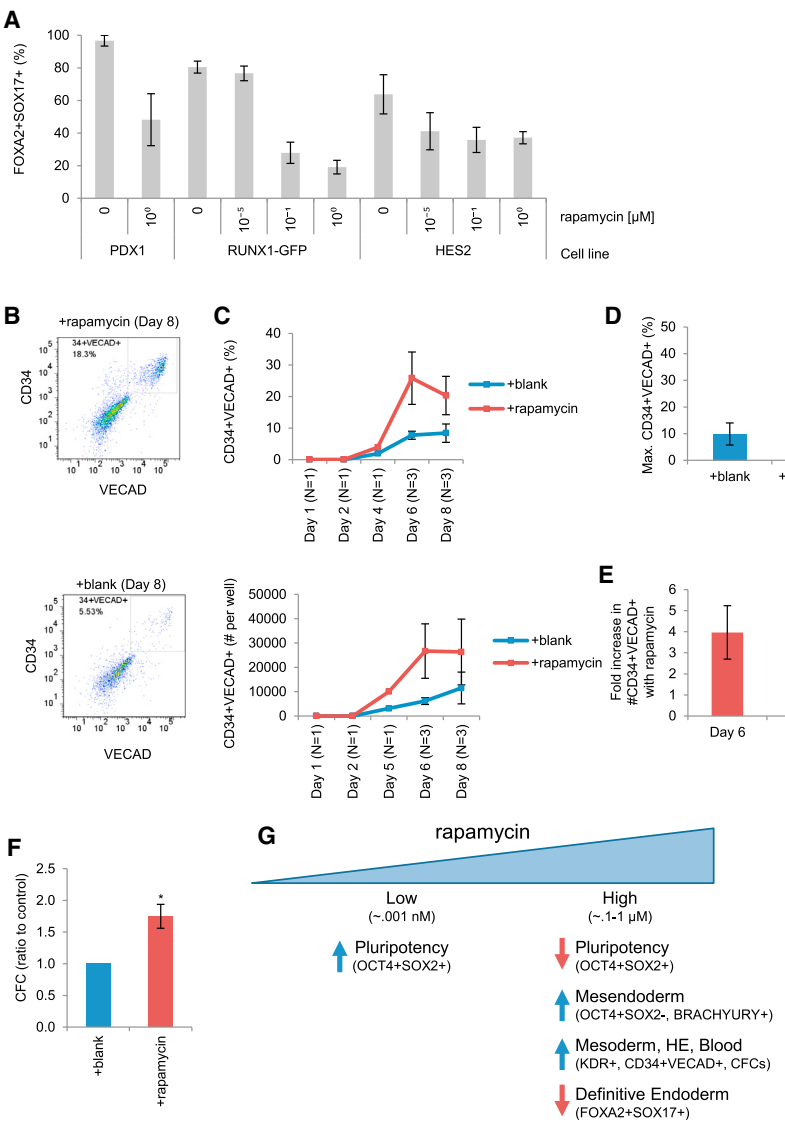

Figure 6. mTOR Inhibition Enhances HE and Blood Induction

(A) Four hPSC cell lines were differentiated to DE using a 5-day protocol and analyzed for $FOXA2^+SOX17^+$ expression. Rapamycin was added as indicated during the D0 phase. n = 3 independent biological replicates. Error bars indicate SD.

(B) Representative flow cytometry scatterplots of VECAD and CD34 expression in day 8 hPSC-derived HE with (top) and without (bottom) rapamycin.

(C) Time course showing $VECAD^+CD34^+$ cells from days 1–8 of differentiation showing percentage (top) and number per well (bottom) with and without rapamycin. N indicates number of independent biological replicates. Error bars indicate SD.

(D) Comparison of the maximum $VECAD^+$ $CD34^+$ percentage obtained with or without rapamycin. *p < 0.05; n = 3 independent biological replicates. Error bars indicate SD.

(E) Comparison of the fold increase in number of $CD34^+VECAD^+$ achieved with rapamycin relative to without rapamycin, on days 6 and 8. n = 3 independent biological replicates. Error bars indicate 99% confidence interval.

(F) CFC comparison of definitive blood obtained with and without rapamycin. n = 3 independent runs of the HES2 (one replicate) and RUNX1-GFP (two replicates) cell lines. Error bars indicate SD. *p < 0.05 (paired Student's t test).

(G) Summary of the role of rapamycin in hPSCs.

See also Figure S6.

DISCUSSION

We have applied an engineered micro-environment based HTS platform to screen a kinase inhibitor library simultaneously for regulators of PSCs, NE, and mesendoderm. Small-molecule control of cell fate is attractive for scale-up purposes, and a focused library could be instrumental in elucidating endogenous regulators of hPSC fate decisions. In line with a previous screen (Desbordes et al., 2008), we found no single compound able to maintain long-term pluripotency, indicating that exogenous pathway agonists or possibly combinations of small-molecule inhibitors may be required for hPSC maintenance. Our multi-lineage readout enabled the discovery of specific pathways endogenously activated in hPSCs amenable to small-molecule control of lineage-specific differentiation. Patterning enabled a more rapid (48 hr versus 7 days) assay and robust response than non-pattern-based screens (Desbordes et al., 2008). Additionally, the short assay duration limits the number of emergent subpopulations, allowing simultaneous detection of these subpopulations to be tracked by OCT4 and SOX2 costaining. In conjunction with cell-number readouts, selection and induction events can be reasonably discriminated.

Our analysis revealed that mTOR inhibitors added alone to SF-defined medium can induce mesendoderm, and our follow-up studies confirmed that rapamycin enhances the formation of HE and blood progenitors. Ten-point dose curves revealed a bimodal effect where rapamycin at low concentrations mildly enhances the purity and number

of $OCT4^+SOX2^+$ PSCs, and higher concentrations reduce the $OCT4^+SOX2^+$ population and enhance mesendoderm differentiation. These results reconcile two previous studies: in line with Easley et al. (2010) we observe no negative effect on pluripotency of rapamycin at low concentrations, and in line with Zhou et al. (2009) we observe loss of pluripotency and induction of mesendoderm at higher concentrations. In contrast to Zhou et al., we found that rapamycin strongly inhibits DE induction. This difference may be serum mediated or cell-line dependent. Additionally, emerging evidence suggests that separate induction mechanisms may confer distinct mesoderm/endoderm subtype potentials (Mendjan et al., 2014).

Although both GSK3β and mTOR inhibition appear to enhance mesendoderm, rapamycin-treated hPSCs appear to generate significantly higher frequencies of $CD34^+VECAD^+CD73^-$ HE phenotype cells compared with CHIR99021 (GSK3β inhibitor)-treated conditions. GSK3β inhibition has been reported to direct hPSC differentiation to blood progenitor (Sturgeon et al., 2014) and cardiac cells (Lian et al., 2012), supporting its role as a driver of lateral plate-derived tissues. Our results indicate that mTOR inhibition is an efficient driver of hPSC differentiation to blood progenitor competent mesoderm. Comparing the mesendoderm subtypes that emerge in GSK3β- and mTOR-inhibited differentiation conditions is an important future direction of our study.

The observation that subnanomolar concentrations of rapamycin have a moderate enhancing effect on pluripotency corresponds with findings of He et al. (2012) showing that rapamycin at 0.01 and 0.03 nM enhances mouse somatic cell reprogramming efficiency nearly 2-fold while concentrations of 0.05 nM or greater have no effect or reduce reprogramming efficiency. Autophagy regulates homeostasis of pluripotency-associated transcription factors including OCT4 in hPSCs, with autophagy inhibition increasing transcription factor levels yet leading to differentiation (Cho et al., 2014). Accordingly, low levels of mTOR inhibition may inhibit autophagy and enhance OCT4 levels in hPSCs sufficiently to enhance pluripotency, with higher levels of mTOR inhibition increasing OCT4 levels beyond a threshold to initiate differentiation. Alternatively, given that differentiated cell types such as hPSC-derived extra-embryonic endoderm are known to inhibit pluripotency (Peerani et al., 2007), it may be that rapamycin selectively inhibits these cell types, leading to increased hPSC numbers. Another possibility is that the cell-fate effects of discrete mTOR inhibition levels may be directly mediated by differential SMAD activation, as mTORC1 inhibition activates SMAD1 and SMAD5 in human prostate cancer cells (Wahdan-Alaswad et al., 2012), and mTORC2 inhibition can enhance SMAD2 and SMAD3 activity via regulation of the SMAD2/3-T220/T179 linker residue (Yu et al., 2015). Understanding the complex interplay between discrete levels of mTOR signaling, autophagy, pluripotency transcription factor homeostasis, signaling pathway activation, and effects on cell-fate choice and subpopulation dynamics remains an important direction of future studies.

The methods we present here are applicable to systems with heterogeneous subpopulations and complex micro-environmental regulation, such as in vitro stem cell and cancer models, and can be applied iteratively. Changes in micro-environmental cues have been attributed to cell-fate transitions (Bonfanti et al., 2010), and heterogeneity in micro-environmental context (such as population size, local cell density, and relative cell position) can deterministically explain phenotypic variance (Snijder et al., 2009). Improved techniques to control the cellular micro-environment in conjunction with improved single-cell analytics will further develop our understanding of molecular cell-fate regulation.

EXPERIMENTAL PROCEDURES

Cell Culture

We obtained hESC lines H9 (WA09) and H7 (WA07) from the WiCell Research Institute, and HES3-RUNX1-GFP (HES3-derived RUNX1-GFP) from A. Elefanty (Monash University). All experiments were performed with H9 unless stated otherwise. These cell lines were cultured according to previously published methods (Nazareth et al., 2013). All cell stocks tested negative for mycoplasma contamination. See Supplemental Experimental Procedures for additional cell line information.

Micro-Patterning hPSCs onto 96-Well Plates and Application of Small Molecules or Controls

We patterned hPSCs on Matrigel into standard 96-well plates as previously described (Nazareth et al., 2013) (see Supplemental Experimental Procedures). Dissociation of hPSCs was performed using TrypLE for 3 min. TrypLE was inactivated with medium containing 20% KO-serum replacement (Invitrogen). Cells were centrifuged and resuspended in NutriStem (NS; StemGent 001-0005) and 10 μM ROCK inhibitor Y-27632. Cells were seeded at 10^5 cells per well (or as described in the text) into 96-well plates, coated with either patterned or non-patterned Matrigel, and incubated for 6 hr. Cells were then washed twice with PBS and incubated for 42 hr in fresh test medium (SF supplemented with growth factors or small molecules, or CM). SF medium consists of DMEM/F12, 1× non-essential amino acids, 50 U ml^{-1} penicillin, 50 μg ml^{-1} streptomycin, 10 μg ml^{-1} bovine transferrin, 0.1 mM β-mercaptoethanol (all Invitrogen), 2% fatty acid-free Cohn's fraction V BSA (Serologicals), 1× trace elements A, B, and C (Mediatech), 50 μg ml^{-1} ascorbic acid (Sigma), and 7 μg ml^{-1} recombinant human insulin. The 400-compound library was obtained from the Ontario Institute of Cancer Research (OICR) (Tables S2 and S3). The following control conditions were included on each 96-well plate: blank (SF medium with no added factors), CM, B (100 ng ml^{-1} BMP4),

BA (10 ng ml^{-1} BMP4 and 100 ng ml^{-1} activin A), and TiF (40 ng ml^{-1} FGF2 and 10 μM SB431542).

Immunocytochemistry and High-Content Image Analysis

Immunocytochemistry was performed as previously described (Nazareth et al., 2013; see also Supplemental Experimental Procedures). Single-cell x-y-coordinate and protein-expression data were exported in tab-delimited text files and imported into in-house software, ContextExplorer (Joel E.E. Ostblom, E.J.P.N., and P.W.Z., unpublished data) for exploration of colony-level details. For figures, 16-bit TIFF images were obtained for each channel, identical contrast adjustment was performed on all controls, and channels were combined into pseudo-colored composite images.

96-Well siRNA Transfection

Human PSCs were first seeded into non-patterned MG-treated 96-well plates at 25,000 cells per well in NS, and incubated for 48 hr. For siRNA transfection, Lipofectamine RNAiMAX transfection reagent (Invitrogen) was used as per manufacturer's instructions, adapted for hPSCs and 96-well plates (see Supplemental Experimental Procedures).

Viability Analysis

To assess viability, we modified the patterned hPSC assay as follows. Instead of fixing at 48 hr, calcein AM (Invitrogen) (1:1,000) and Hoechst 33342 (1:1,000) were added directly to the medium, incubated for 30 min, and then imaged.

Differentiation of hPSCs toward Blood Progenitors and Definitive Endoderm

For ultra-high-throughput production of size-specified cell aggregates, 400-μm diameter micro-well plates (commercially available as Aggrewells, STEMCELL Technologies) were manufactured in-house in 24-well plates (Ungrin et al., 2008). For depletion of MEFs, hPSCs were dissociated with TrypLE and plated onto Geltrex (diluted 1:50) for 48 hr in NS. After 48 hr, TrypLE was added for 5 min and then quenched with 50% fetal bovine serum in DMEM/F12. The resulting single-cell suspension was seeded at 6×10^5 cells per well of a micro-well plate (500 cells per aggregate) in the presence of Y-27632 (for 24 hr) at 1,500 rpm for 5 min. Aggregates were cultured in hypoxia for 8 days in base medium supplemented with cytokines BMP4 (40 ng ml^{-1}, R&D Systems), vascular endothelial growth factor (VEGF) (50 ng ml^{-1}, R&D), SCF (40 ng ml^{-1}, R&D), basic FGF (5 ng ml^{-1}, Peprotech), and rapamycin (0.1 μM, Sigma). Note that rapamycin is highly labile, and we recommend minimizing freeze-thaw cycles and titrating for maximum effect. The base medium consists of StemPro34 (Invitrogen), ascorbic acid (50 μg ml^{-1}, Sigma), L-glutamine (1% v/v, Invitrogen), penicillin/streptomycin (1% v/v, Invitrogen), 1-monothioglycerol (4×10^{-4} M, Sigma), and transferrin (150 μg ml^{-1}, Roche). On day 2, hPSC-derived cells were transferred to low-cluster six-well plates, in medium without rapamycin, and cultured for an additional 6 days shaken at 85 rpm (Orbi-Shaker XL, Benchmark Scientific). Endoderm induction to $FOXA2^+SOX17^+$ DE was performed as previously described (Rezania et al., 2012).

qRT-PCR

qRT-PCR was performed as described previously (Onishi et al., 2012). In brief, RNA was isolated using the PureLink RNA Mini Kit (Ambion) and reverse transcribed with Superscript III (Life Technologies). PCR was performed on the QuantStudio 6 Flex (Life Technologies) using SYBR Master Mix (Roche) and primers provided by the Center for Commercialization of Regenerative Medicine. Gene NCBI-RefSeq accession numbers are provided in Table S4.

CFC Assay

A minimum of 1.5×10^5 cells were seeded on day 8 in 35-mm Greiner dishes in methylcellulose-based MethoCult H4435 Enriched medium (STEMCELL). Samples were scored based on morphology 14 days after plating as described by technical manuals provided by STEMCELL.

Statistical Analysis

Statistics were computed using one-way ANOVA, two-factor ANOVA, or linear regression as indicated. All statistics were computed in MATLAB using p values as indicated. N values are independent replicates, not technical replicates, except where noted. Enrichment analysis was performed using the hypergeometric distribution in Microsoft Excel. Z′ factor was used to assess assay quality (Zhang et al., 1999). Z′ is defined as $Z' = 1 - (3\sigma_{positive} + 3\sigma_{negative})/|\mu_{positive} - \mu_{negative}|$, where μ and σ are the mean and SD of the positive (CM-treated) and negative (BMP4-treated) control as labeled. Hierarchical clustering was performed with MeV (MultiExperiment Viewer, http://www.tm4.org/) using Euclidan distance as the similarity metric (centered) and centroid linkage as the clustering method. Exploratory analysis was performed with Microsoft Excel and Tableau (Tableau Software, www.tableau.com).

SUPPLEMENTAL INFORMATION

Supplemental Information includes Supplemental Experimental Procedures, six figures and four tables and can be found with this article online at http://dx.doi.org/10.1016/j.stemcr.2016.04.003.

AUTHOR CONTRIBUTIONS

E.N. designed, performed, and analyzed most experiments. N.R. performed all blood-induction experiments. T.Y. provided cell-culture support. M.P. and R.A. provided the kinase inhibitor library and related support. E.N. and P.W.Z. designed the project and wrote the manuscript.

ACKNOWLEDGMENTS

This work is funded by the Canadian Institutes of Health Research (CIHR) (P.W.Z). E.J.P.N. is supported by a CIHR Frederick Banting and Charles Best Canada Graduate Scholarships Doctoral Award. P.W.Z. is the Canada Research Chair in Stem Cell Bioengineering. We thank Michael Prakesch and Rima Al-awar (Ontario Institute of Cancer Research) for providing the kinase inhibitor library, Jennifer Ma for creating the graphical abstract, Celine Bauwens for

editing assistance, and the Centre for Commercialization of Regenerative Medicine for all primers.

Received: September 3, 2015
Revised: April 4, 2016
Accepted: April 4, 2016
Published: April 28, 2016

REFERENCES

Bonfanti, P., Claudinot, S., Amici, A.W., Farley, A., Blackburn, C.C., and Barrandon, Y. (2010). Microenvironmental reprogramming of thymic epithelial cells to skin multipotent stem cells. Nature *466*, 978–982.

Cai, J., Yu, C., Liu, Y., Chen, S., Guo, Y., Yong, J., Lu, W., Ding, M., and Deng, H. (2009). Generation of homogeneous PDX1(+) pancreatic progenitors from human ES cell-derived endoderm cells. J. Mol. Cell Biol. *2*, 50–60.

Chambers, S.M., Fasano, C.A., Papapetrou, E.P., Tomishima, M., Sadelain, M., and Studer, L. (2009). Highly efficient neural conversion of human ES and iPS cells by dual inhibition of SMAD signaling. Nat. Biotechnol. *27* (3), 275–280.

Cho, Y.H., Han, K.M., Kim, D., Lee, J., Lee, S.H., Choi, K.W., Kim, J., and Han, Y.M. (2014). Autophagy regulates homeostasis of pluripotency-associated proteins in hESCs. Stem Cells *32*, 424–435.

Csaszar, E., Kirouac, D.C., Yu, M., Wang, W., Qiao, W., Cooke, M.P., Boitano, A.E., Ito, C., and Zandstra, P.W. (2012). Rapid expansion of human hematopoietic stem cells by automated control of inhibitory feedback signaling. Cell Stem Cell *10*, 218–229.

Desbordes, S.C., Placantonakis, D.G., Ciro, A., Socci, N.D., Lee, G., Djaballah, H., and Studer, L. (2008). High-throughput screening assay for the identification of compounds regulating self-renewal and differentiation in human embryonic stem cells. Cell Stem Cell *2*, 602–612.

Ditadi, A., and Sturgeon, C.M. (2015). Directed differentiation of definitive hemogenic endothelium and hematopoietic progenitors from human pluripotent stem cells. Methods. http://dx.doi.org/10.1016/j.ymeth.2015.10.001.

Easley, C.A.t., Ben-Yehudah, A., Redinger, C.J., Oliver, S.L., Varum, S.T., Eisinger, V.M., Carlisle, D.L., Donovan, P.J., and Schatten, G.P. (2010). mTOR-mediated activation of p70 S6K induces differentiation of pluripotent human embryonic stem cells. Cell Reprogram. *12*, 263–273.

Eilken, H.M., Nishikawa, S., and Schroeder, T. (2009). Continuous single-cell imaging of blood generation from haemogenic endothelium. Nature *457*, 896–900.

Greber, B., Coulon, P., Zhang, M., Moritz, S., Frank, S., Muller-Molina, A.J., Arauzo-Bravo, M.J., Han, D.W., Pape, H.C., and Scholer, H.R. (2011). FGF signalling inhibits neural induction in human embryonic stem cells. EMBO J. *30*, 4874–4884.

Haibe-Kains, B., El-Hachem, N., Birkbak, N.J., Jin, A.C., Beck, A.H., Aerts, H.J., and Quackenbush, J. (2013). Inconsistency in large pharmacogenomic studies. Nature *504*, 389–393.

He, J., Kang, L., Wu, T., Zhang, J., Wang, H., Gao, H., Zhang, Y., Huang, B., Liu, W., Kou, Z., et al. (2012). An elaborate regulation of Mammalian target of rapamycin activity is required for somatic cell reprogramming induced by defined transcription factors. Stem Cells Dev. *21*, 2630–2641.

Kim, D.S., Lee, J.S., Leem, J.W., Huh, Y.J., Kim, J.Y., Kim, H.S., Park, I.H., Daley, G.Q., Hwang, D.Y., and Kim, D.W. (2010). Robust enhancement of neural differentiation from human ES and iPS cells regardless of their innate difference in differentiation propensity. Stem Cell Rev. *6*, 270–281.

Lamming, D.W., Ye, L., Katajisto, P., Goncalves, M.D., Saitoh, M., Stevens, D.M., Davis, J.G., Salmon, A.B., Richardson, A., Ahima, R.S., et al. (2012). Rapamycin-induced insulin resistance is mediated by mTORC2 loss and uncoupled from longevity. Science *335*, 1638–1643.

Lian, X., Hsiao, C., Wilson, G., Zhu, K., Hazeltine, L.B., Azarin, S.M., Raval, K.K., Zhang, J., Kamp, T.J., and Palecek, S.P. (2012). Robust cardiomyocyte differentiation from human pluripotent stem cells via temporal modulation of canonical Wnt signaling. Proc. Natl. Acad. Sci. USA *109*, E1848–E1857.

Maherali, N., and Hochedlinger, K. (2008). Guidelines and techniques for the generation of induced pluripotent stem cells. Cell Stem Cell *3*, 595–605.

Mendjan, S., Mascetti, V.L., Ortmann, D., Ortiz, M., Karjosukarso, D.W., Ng, Y., Moreau, T., and Pedersen, R.A. (2014). NANOG and CDX2 pattern distinct subtypes of human mesoderm during exit from pluripotency. Cell Stem Cell *15*, 310–325.

Nazareth, E.J., Ostblom, J.E., Lucker, P.B., Shukla, S., Alvarez, M.M., Oh, S.K., Yin, T., and Zandstra, P.W. (2013). High-throughput fingerprinting of human pluripotent stem cell fate responses and lineage bias. Nat. Methods *10*, 1225–1231.

Nostro, M.C., Sarangi, F., Ogawa, S., Holtzinger, A., Corneo, B., Li, X., Micallef, S.J., Park, I.H., Basford, C., Wheeler, M.B., et al. (2011). Stage-specific signaling through TGFbeta family members and WNT regulates patterning and pancreatic specification of human pluripotent stem cells. Development *138*, 861–871.

Onishi, K., Tonge, P.D., Nagy, A., and Zandstra, P.W. (2012). Microenvironment-mediated reversion of epiblast stem cells by reactivation of repressed JAK-STAT signaling. Integr. Biol. (Camb) *4*, 1367–1376.

Peerani, R., Rao, B.M., Bauwens, C., Yin, T., Wood, G.A., Nagy, A., Kumacheva, E., and Zandstra, P.W. (2007). Niche-mediated control of human embryonic stem cell self-renewal and differentiation. EMBO J. *26*, 4744–4755.

Pick, M., Azzola, L., Mossman, A., Stanley, E.G., and Elefanty, A.G. (2007). Differentiation of human embryonic stem cells in serum-free medium reveals distinct roles for bone morphogenetic protein 4, vascular endothelial growth factor, stem cell factor, and fibroblast growth factor 2 in hematopoiesis. Stem Cells *25*, 2206–2214.

Rezania, A., Bruin, J.E., Riedel, M.J., Mojibian, M., Asadi, A., Xu, J., Gauvin, R., Narayan, K., Karanu, F., O'Neil, J.J., et al. (2012). Maturation of human embryonic stem cell-derived pancreatic progenitors into functional islets capable of treating pre-existing diabetes in mice. Diabetes *61*, 2016–2029.

Sabatini, D.M. (2006). mTOR and cancer: insights into a complex relationship. Nat. Rev. Cancer *6*, 729–734.

Sabers, C.J., Martin, M.M., Brunn, G.J., Williams, J.M., Dumont, F.J., Wiederrecht, G., and Abraham, R.T. (1995). Isolation of a

protein target of the FKBP12-rapamycin complex in mammalian cells. J. Biol. Chem. *270*, 815–822.

Shalaby, F., Ho, J., Stanford, W.L., Fischer, K.D., Schuh, A.C., Schwartz, L., Bernstein, A., and Rossant, J. (1997). A requirement for Flk1 in primitive and definitive hematopoiesis and vasculogenesis. Cell *89*, 981–990.

Singh, A.M., Reynolds, D., Cliff, T., Ohtsuka, S., Mattheyses, A.L., Sun, Y., Menendez, L., Kulik, M., and Dalton, S. (2012). Signaling network crosstalk in human pluripotent cells: a Smad2/3-regulated switch that controls the balance between self-renewal and differentiation. Cell Stem Cell *10*, 312–326.

Smith, J.R., Vallier, L., Lupo, G., Alexander, M., Harris, W.A., and Pedersen, R.A. (2008). Inhibition of Activin/Nodal signaling promotes specification of human embryonic stem cells into neuroectoderm. Dev. Biol. *313*, 107–117.

Snijder, B., Sacher, R., Ramo, P., Damm, E.M., Liberali, P., and Pelkmans, L. (2009). Population context determines cell-to-cell variability in endocytosis and virus infection. Nature *461*, 520–523.

Snijder, B., Sacher, R., Ramo, P., Liberali, P., Mench, K., Wolfrum, N., Burleigh, L., Scott, C.C., Verheije, M.H., Mercer, J., et al. (2012). Single-cell analysis of population context advances RNAi screening at multiple levels. Mol. Syst. Biol. *8*, 579.

Sturgeon, C.M., Ditadi, A., Awong, G., Kennedy, M., and Keller, G. (2014). Wnt signaling controls the specification of definitive and primitive hematopoiesis from human pluripotent stem cells. Nat. Biotechnol. *32*, 554–561.

Sun, N., Yazawa, M., Liu, J., Han, L., Sanchez-Freire, V., Abilez, O.J., Navarrete, E.G., Hu, S., Wang, L., Lee, A., et al. (2012). Patient-specific induced pluripotent stem cells as a model for familial dilated cardiomyopathy. Sci. Transl Med. *4*, 130ra147.

Tsutsui, H., Valamehr, B., Hindoyan, A., Qiao, R., Ding, X., Guo, S., Witte, O.N., Liu, X., Ho, C.M., and Wu, H. (2011). An optimized small molecule inhibitor cocktail supports long-term maintenance of human embryonic stem cells. Nat. Commun. *2*, 167.

Ungrin, M.D., Joshi, C., Nica, A., Bauwens, C., and Zandstra, P.W. (2008). Reproducible, ultra high-throughput formation of multicellular organization from single cell suspension-derived human embryonic stem cell aggregates. PLoS One *3*, e1565.

Vallier, L., Reynolds, D., and Pedersen, R.A. (2004). Nodal inhibits differentiation of human embryonic stem cells along the neuroectodermal default pathway. Dev. Biol. *275*, 403–421.

Vallier, L., Alexander, M., and Pedersen, R.A. (2005). Activin/Nodal and FGF pathways cooperate to maintain pluripotency of human embryonic stem cells. J. Cell Sci. *118*, 4495–4509.

Vallier, L., Touboul, T., Brown, S., Cho, C., Bilican, B., Alexander, M., Cedervall, J., Chandran, S., Ahrlund-Richter, L., Weber, A., et al. (2009). Signaling pathways controlling pluripotency and early cell fate decisions of human induced pluripotent stem cells. Stem Cells *27*, 2655–2666.

Wahdan-Alaswad, R.S., Bane, K.L., Song, K., Shola, D.T., Garcia, J.A., and Danielpour, D. (2012). Inhibition of mTORC1 kinase activates Smads 1 and 5 but not Smad8 in human prostate cancer cells, mediating cytostatic response to rapamycin. Mol. Cancer Res. *10*, 821–833.

Yu, P., Pan, G., Yu, J., and Thomson, J.A. (2011). FGF2 sustains NANOG and switches the outcome of BMP4-induced human embryonic stem cell differentiation. Cell Stem Cell *8*, 326–334.

Yu, J.S., Ramasamy, T.S., Murphy, N., Holt, M.K., Czapiewski, R., Wei, S.K., and Cui, W. (2015). PI3K/mTORC2 regulates TGF-beta/Activin signalling by modulating Smad2/3 activity via linker phosphorylation. Nat. Commun. *6*, 7212.

Zhang, J.H., Chung, T.D., and Oldenburg, K.R. (1999). A simple statistical parameter for use in evaluation and validation of high throughput screening assays. J. Biomol. Screen. *4*, 67–73.

Zhang, P., Li, J., Tan, Z., Wang, C., Liu, T., Chen, L., Yong, J., Jiang, W., Sun, X., Du, L., et al. (2008). Short-term BMP-4 treatment initiates mesoderm induction in human embryonic stem cells. Blood *111*, 1933–1941.

Zhou, J., Su, P., Wang, L., Chen, J., Zimmermann, M., Genbacev, O., Afonja, O., Horne, M.C., Tanaka, T., Duan, E., et al. (2009). mTOR supports long-term self-renewal and suppresses mesoderm and endoderm activities of human embryonic stem cells. Proc. Natl. Acad. Sci. USA *106*, 7840–7845.